Electronic Supplementary Material (ESI) for ChemComm.

Supporting Information

Reducing volume expansion in micro silicon anodes via aramid nanofibers for stable lithium-ion batteries

Qingqing Liu [a], Wei Tang [a], Chen Yang [a], Wenlong Cai[b,], Feng Chen[a,] *, Qiang Fu [a].*

[a] College of Polymer Science & Engineering, State Key Laboratory of Polymer Materials Engineering, Sichuan University, Cheng Du, 610065, PR China.

[b] Department of Advanced Energy Materials, College of Materials Science and Engineering, Sichuan University, Chengdu, 610064, P. R. China.

∗ Corresponding author. Wenlong Cai, Feng Chen

E-mail addresses: caiwl@scu.edu.cn (W. Cai); fengchen@scu.edu.cn (F. Chen).

Table of contents

1. Experimental section

1.1 Materials and equipment.

Aramid fiber Kevlar 49 was provided by DuPont (USA). Dimethyl sulfoxide (DMSO, AR), and potassium hydroxide (KOH, AR) were ordered from Kermal Chemical Reagent (China). Hydrochloric acid (HCl, AR) and tert-butylalcohol (AR) were purchased from Chengdu Kelong Chemical (China). The original compositing silicon was obtained from BTR New Material Group (China). A polypropylene (PP) porous separator (Celgrad 2400) with a thickness of 25 μm was purchased from Shenzhen Xinyuan New Energy Material (China). Liquid electrolyte, 1.0 M lithium hexafluorophosphate (LiPF6) in a 1:1 mixture of ethylene carbonate (EC) and dimethyl carbonate (DMC) containing 5.0 wt.% fluoroethylene carbonate (FEC), was provided by Guangdong Canrd New Energy Technology (China). Acetylene black, lithium polyacrylate (PAALi), copper foil, button battery case, lithium metal sheet, and conductive carbon black were purchased from Guangdong Canrd New Energy Technology (China). Deionized water was provided through a MilliQ system.

1.2 Fabrication of aramid nanofiber solutions.

The dispersion of ANFs was generated based on the strategy reported by Kotov's group.[1] Kevlar 49 aramid fibers (7.0 g) and KOH (7.0 g) were added into DMSO (500 ml) to prepare the ANF dispersion after mechanical stirring (room temperature, 168 h). The electrostatic repulsion between ANFs ensured a stable dispersion. The residual Kevlar 49 fibers and KOH in ANF dispersion were removed by centrifugation (8000 rpm, 1 h).[2]

1.3 Preparation of SMP coating with ANFs.

SMPs (5 g) were added to a batch of diluted ANF dispersion (10 g), and the different dilution ratios are calculated according to the mass loading of ANFs in the composites. The mixture of ANFs and SMPs was then placed in a blender to increase uniformity, thus forming the ANF coating on the surface of the SMPs. The ANF-SMP mixture was frozen into the solid state using liquid N_2, and the ANFs were immobilized on the surface of the SMPs. And the frozen mixture was then immersed in a coagulation bath for 72 h. The coagulation bath, which consisted of 320 g deionized water, 80 g tert-butylalcohol, and 2 g HCl, was changed every 24 h. After the coagulation bath process, these samples were again frozen by liquid N_2 and freeze-drying for 120 h to remove the residual solvent.

1.4 Preparation of electrodes.

The as-prepared dry mixture was ground into microparticles to make electrodes. The active material (SMPs with different mass loadings of ANFs), conductive agent (acetylene black), and binder (PAALi) were mixed at a mass ratio of 75:15:10. During the preparation process of the slurry, deionized water was added to the mixture at a mass ratio of 1:1 for better fluidity to maintain the solid content at 22.7 %. After the slurries were coated on the copper foil in an 80 μm thickness, they were dried in a vacuum (80 °C, 12 h) to obtain the electrodes. The prepared electrodes were cut into 12 mm disks that serve as the anode in half-cell and have an areal active mass loading of 1–1.5 mg cm^{-2}

1.5 Characterization

The morphologies and thickness of the samples were observed using a scanning electron microscopy (SEM) system (Inspect F50, USA). The samples are freeze-dried and then received a gold coating in a vacuum before SEM observation. The prepared ANFs dispersion was observed using a transmission electron microscopy (TEM) system (H-600, Japan) at 20 kV. The diluted dispersion (0.005 wt%) was dropped on a copper net and then dried in a vacuum before TEM observation. X-ray photoelectron spectroscopy (XPS) of the original materials and prepared composites were obtained using an electron spectrometer (Kratas AXIS SUPRA, Thermo Scientific, USA). Raman spectra were obtained using a Raman system (Renishaw inVia Reflex, USA) with 532 nm excitation. Fourier transform infrared spectroscopy (FT-IR) was obtained on a spectrometer (Bruker VERTEX 70, German) using a KBr pellet method. The wide-angle X-ray diffraction (WXRD) patterns were collected using a diffractometer (Ultima IV, Japan) with Cu $K\alpha_1$ radiation (λ = 1.5406 Å) to characterize the crystal structure variation of the SMP and 0.2ANF-SMP. The mechanical properties including tensile strengths, moduli, and elongations-at-break of the ANF films were determined using a dynamic mechanical analyzer (IMSTRON 5967, USA). Rectangular strips (20 mm in length, 5 mm in width) of the samples were prepared for the measurement, and the reported values were the averages of at least five replicates for each sample.

The nanoindentation of the electrodes was measured using a nanoindenter (Hysitron TI 980, Bruker, German) at a speed of 3000 nm min^{-1}.[3] A drop shape analysis system (DSA 100, KRUSS, Germany) was used in the analysis of static contact angles to investigate the wettability of the ANF film and PAA film with electrolyte. The electrical

conductivity was measured with a four-probe method using a general-purpose tester (JYC3100). The above electrodes were assembled into the CR2032 coin-type cells with the lithium electrode as the counter electrode in a glove box under an inert atmosphere condition.[4] A PP porous separator (Celgard 2400) was utilized to separate the working and counter electrodes in an electrolyte. The electrochemical impedance spectroscopy (EIS) was performed by using an electrochemical workstation (CHI660E, China) with a DC potential of 5 mV between 0.1 Hz and 1000 kHz. To obtain the cyclic voltammetry (CV) curves, the scan was set at a rate of 1×10^{-4} V s^{-1} in a range of 0.01–1.5 V versus Li/Li^{+} for 3 cycles. The galvanostatic cycling measurements and rate performance were conducted on a CT2001A blue electricity charge and discharge test platform (Wuhan Blue Electronics Technology Co., Ltd) at determinate voltage windows of 0.01–1.5 V. More details of the experiment are available in our previous article.[2]

2. The morphology of ANF dispersion

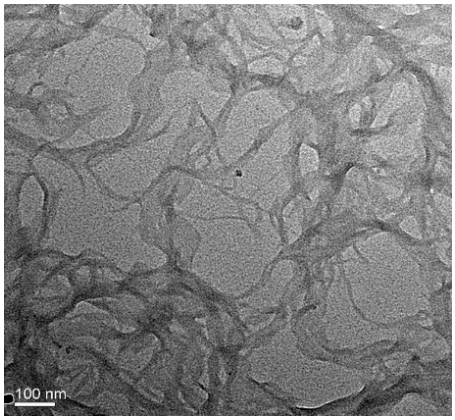

Fig. S1. The TEM image of the ANF dispersion.

The aramid fibers were dissolved in the KOH/DMSO solution to split the large blocks of fibers from macroscale to nanoscale. The morphology of the ANFs prepared in this word is shown in **Figure S1**. The split of macroscale fiber is ascribed to the extraction of hydrogen from amide groups and the significant reduction in the strength of hydrogen bonds between the polymer chains.[1]

3. The morphologies of ANF-SMPs and characterization

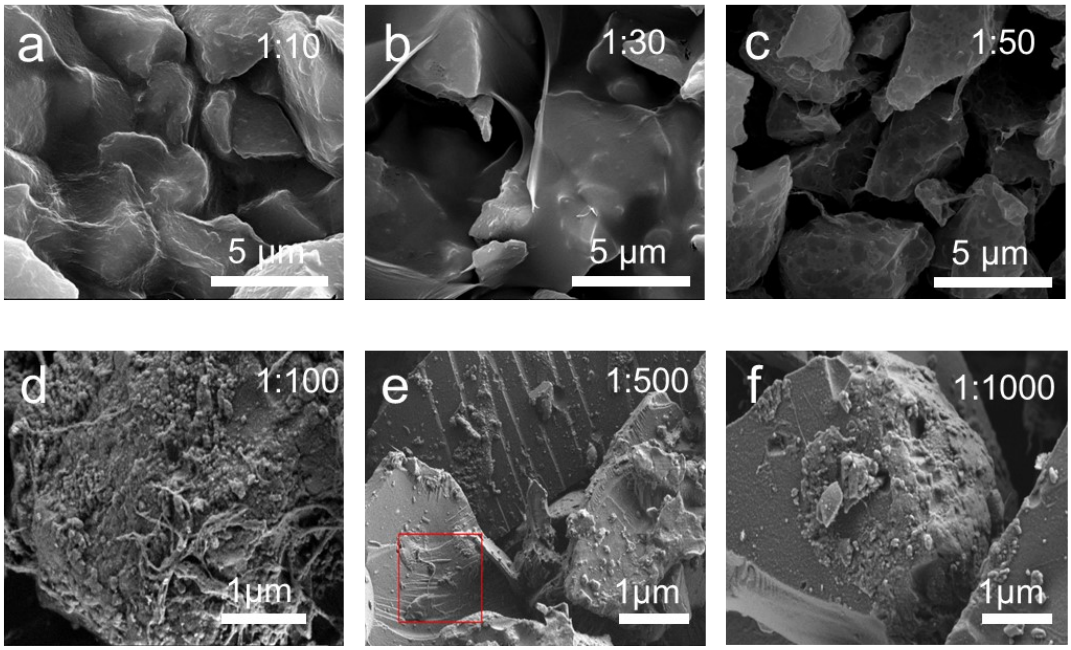

Fig. S2. SEM image of SMP coating with different mass loadings of ANFs.

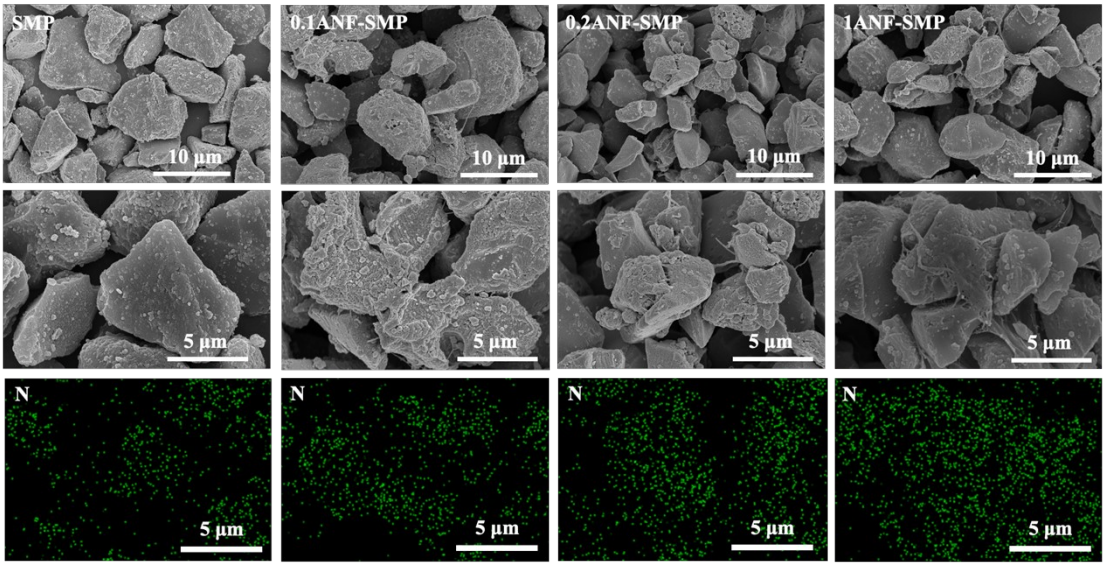

Fig. S3. SEM and EDS images of SMP coating with different mass loadings of ANFs.

We refined the ANF loading range and systematically compared three promising candidates of ANF-SMPs, i.e., 0.1ANF-SMP (0.1 wt%, 1:1000), 0.2ANF-SMP (0.2 wt%, 1:500) and 1ANF-SMP (1 wt%, 1:100). In their surface morphology, the bundle of ANFs became obvious with the increase of ANFs loading. According to the N distribution on the surface shown in EDS images, the density of the N element, which represents the amide group in ANFs, also increases slightly with ANF loadings.

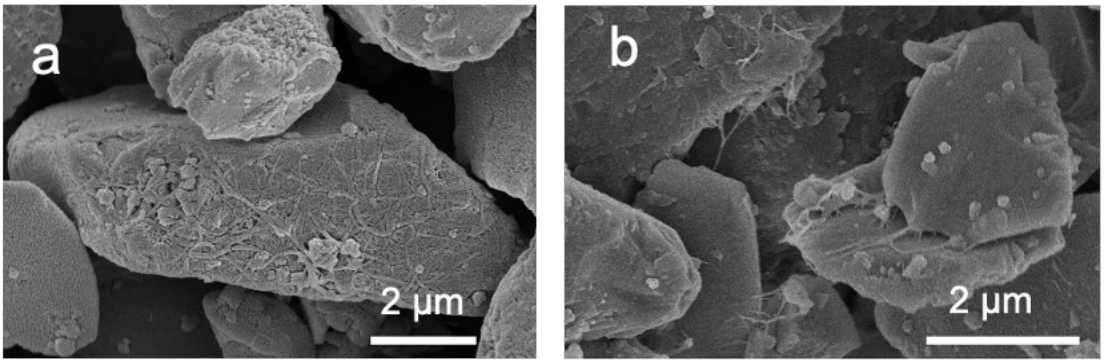

Fig. S4. (a) SEM image of 0.2ANF-SMP. (b) SEM image of 0.2ANF-SMP without coagulation bath.

The ANF coated on the surface of SMP could protonate on the surface of SMP during the coagulation bath, and the fiber would become coarser. Comparing the thickness of ANFs before (Figure S4b) and after (Figure S4a) the protonation, it can be verified that ANFs become thickened through the coagulation bath. The diameter of ANF fiber before the coagulation bath is about 0.04 μm in Figure S4b, while the diameter of ANFs after 3 days coagulation bath is 0.11 μm in Figure S4a. Taking advantage of the mechanical strength of ANFs, the coating of ANFs on ANF-SMP could inhibit the volume expansion of SMP caused by pulverization during the (de)lithiation process.

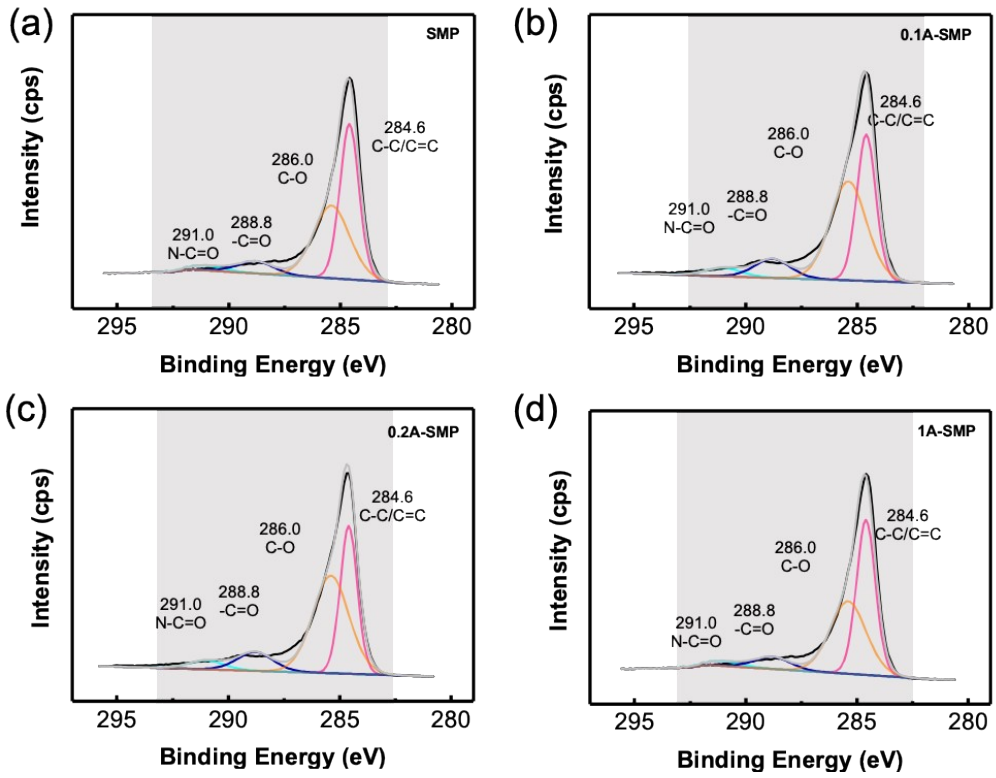

Fig. S5. The XPS C 1s spectra of (a) SMP, (b) 0.1A-SMP, (c) 0.2A-SMP, and (d) 1A-SMP.

More characterizations are conducted to analyze the existence of ANF in composites. Figure 2e and 2f show the full spectra and N element spectra of SMP before and after coating with different mass ratios of ANFs respectively. It's clearly found that the appearance of increasing N element in composite with the increasing ANF loading. Although the mass ratio of ANF to SMP is 1:1000, the N element still could be found in the SMP coating with ANFs, which is probably owing to the effect of 1D-nanostructure of ANFs. The C 1s spectra in Figure S5 reveal four characteristic XPS peaks at the binding energies of 284.6, 286.0, 288.8, and 291.0 eV, corresponding to C-C/C=C, C-O, C=O, and -N-C=O signals, respectively. With the increased mass ratio

of ANFs, the C=O peak becomes wider and the C-O peak tends to be narrower. These results indicate the successful coating and re-protonation of ANFs on SMP.

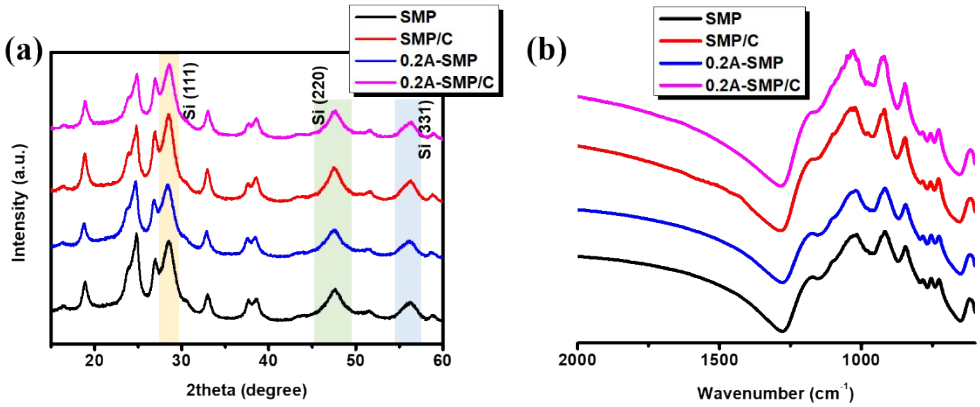

Fig. S6. (a) FTIR spectra and (b) XRD patterns of SMP, SMP/C, 0.2ANF-SMP and 0.2ANF-SMP/C.

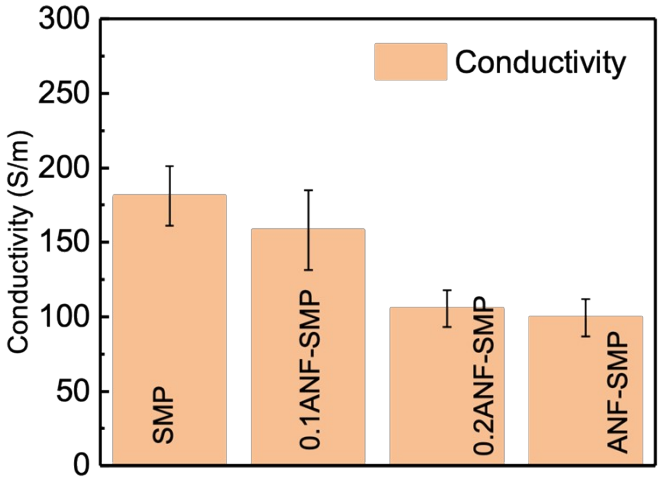

Fig. S7. The conductivity of different ANF-SMP electrodes.

The conductivity of different electrodes was measured by a four-point probe measurement. The conductivity of SMP, 0.1ANF-SMP, 0.2ANF-SMP and ANF-SMP electrodes are 163.97, 158.21, 92.88 and 84.6 S/m, respectively, which is shown in Figure S7. With the increase of ANFs coating on SMP, the conductivity of the electrode gradually decreases due to the insulation of ANFs. Although the expansion can be inhibited by adding more ANFs, the conductivity will become worse, which will also affect the electrochemical stability of SMP electrode. Therefore, it is critical to choose an appropriate mass ratio of ANF: SMP to balance the benefits of reduced volume expansion and the defect caused by poor conductivity. In the cyclic performance tests, we found that 0.2ANF-SMP electrodes showed good cyclic stability, so that a trade-off between volume expansion inhibition and electrochemical performance effects could be achieved at a mass ratio of 1:500 (0.2ANF-SMP).

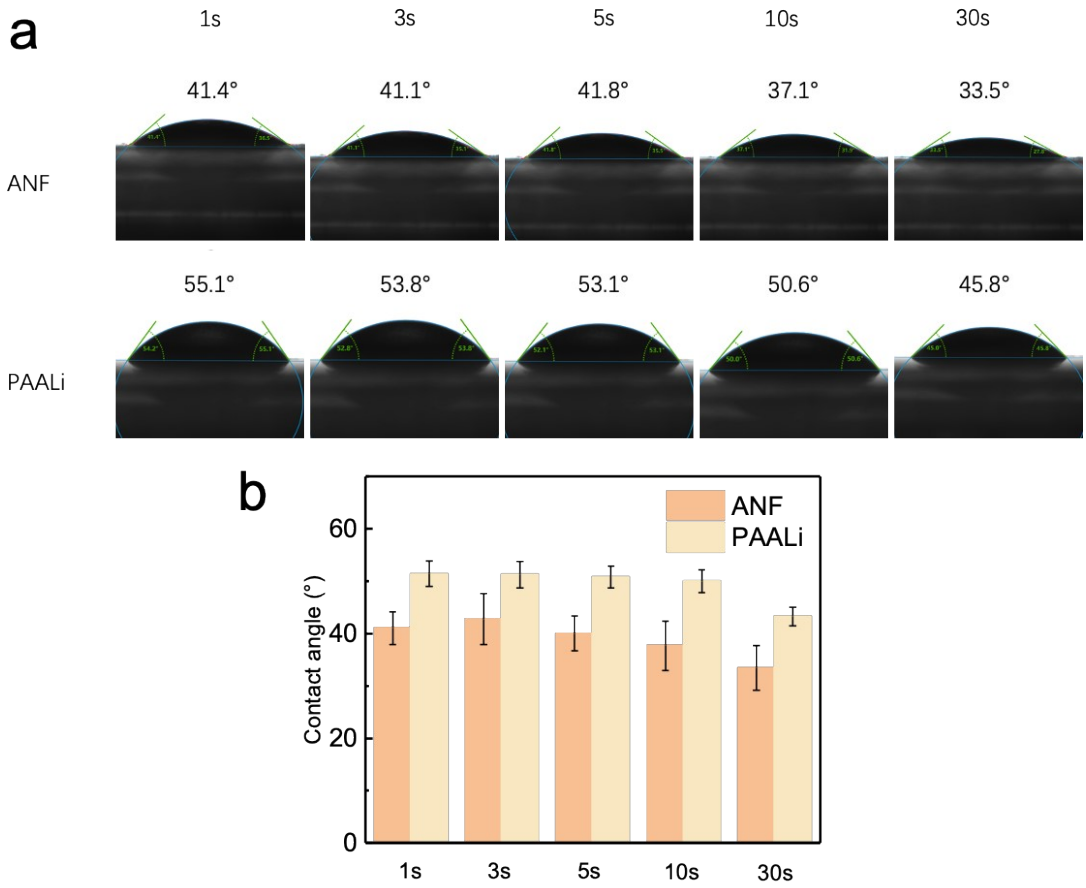

Fig. S8. (a) The contact angle of electrolyte on ANF and PAALi film. (b) The mean bar chart and error bar.

The PAALi solution was the binder we used to prepare the electrode sheet. The addition of ANFs may improve the infiltration of electrolytes to the electrode. We did not directly use the ANF-SMP electrode to measure the contact angles of the electrolyte solvent due to its porous structure. Then the contact angles of electrolyte solvent on the ANF film and PAALi film are compared in Figure S8. The results show that the contact angle of ANF film is smaller than that of PAALi film, indicating that ANF film has better infiltration of electrolytes. So the addition of ANFs could improve the wettability between the electrolyte and silicon particles. With the increase of ANF, the interaction of SMP and electrolytes could be enhanced.

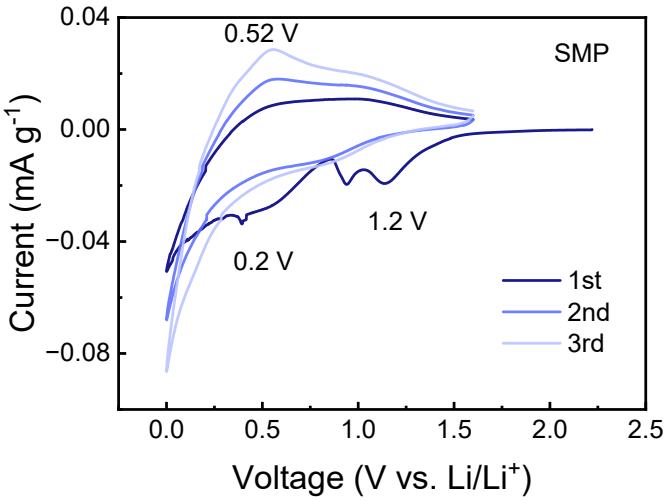

Fig. S9. CV curves of SMP electrode for the first 3 cycles with a scan rate of 0.1 mV s^{-1}.

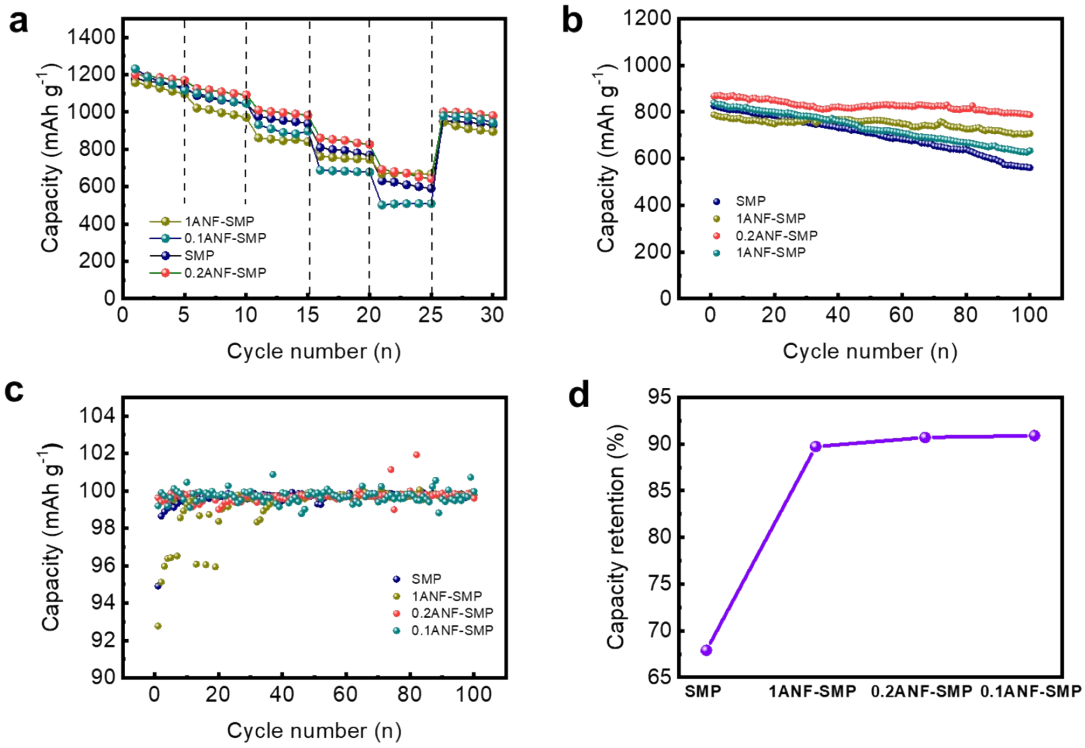

Fig. S10. (a) Rate capabilities of SMP coating with the different mass loadings of ANFs at various current densities. (b) The cycling performance and (c) CE of SMP coating with the different mass loadings of ANFs at 0.5C. (d) The capacity retention of SMP coating with the different mass loading of ANFs.

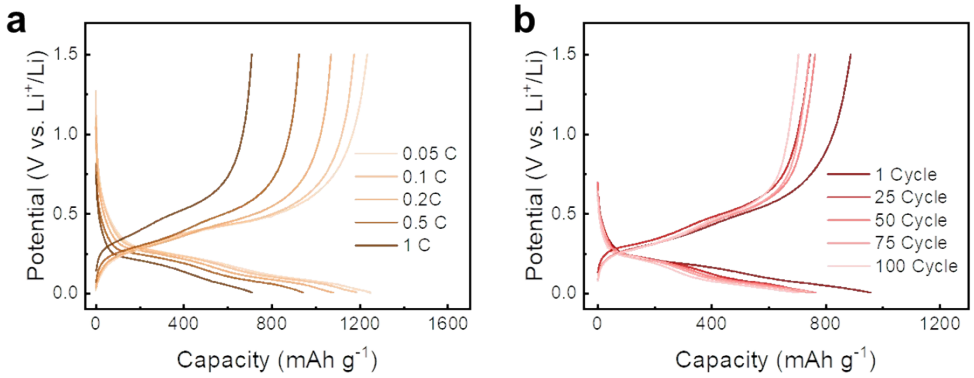

Fig. S11. (a) The discharge-charge curves of 0.2ANF-SMP electrode under the rate performance. (b) The discharge-charge curves of 0.2ANF-SMP electrode at different periods during long cycles.

4. The SEM images of electrodes after the cycling test

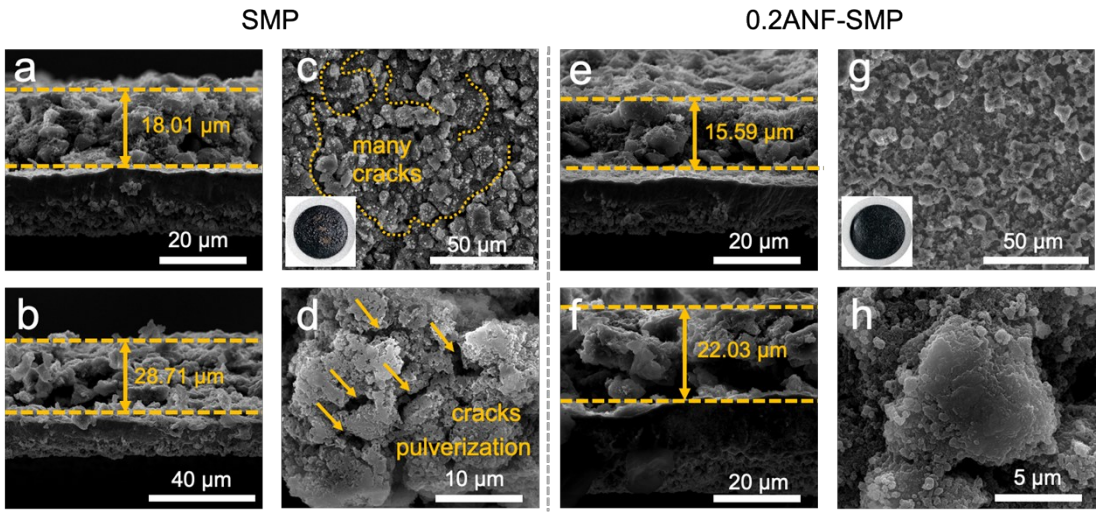

Fig. S12. Cross-sectional SEM images of the pristine SMP and the 0.2ANF-SMP electrodes before (a, e) and after cycling tests (b, f); the surface of the SMP (c, d) and the 0.2ANF-SMP (g, h) electrodes after cycling tests, with the inset images showing electrode sheets after 100 cycles.

The experimental results above indicate the effect of the ANF coating on the micromorphologies and electrochemical performance of electrodes. The major properties of the pristine SMP electrode could be enhanced, which indicates a suitable mass loading of ANFs could effectively stable the SMP electrode. To further verify this conclusion, the half-cell was disassembled after 100 cycles, and the removed anode electrodes were measured for electrode thickness to indicate volume expansion. During the dynamic process, the lithiation would lead to the amorphization of crystalline silicon in the electrode and significant volume changes, resulting in microparticle pulverization.[5] The thickness of the pristine SMP electrode and the 0.2ANF-SMP electrode before and after 100 cycles at a rate of 0.5 C is shown in **Figure S9**. The

thickness of SMP and 0.2ANF-SMP electrodes before cycles are presented in Figure S9a and S9e. After 100 cycles, both SMP and 0.2ANF-SMP have volume expansion, which is shown in the cross-sectional thickness in Figure S9b, S9f. The increased thickness of the 0.2ANF-SMP electrode is only 41.31%, which is lower than that of the pristine SMP electrode (59.41%). Therefore, the 0.2ANF-SMP electrode has a 30.46% decrease in the thickness of electrodes, indicating the inhibition effect on volume expansion during (de)lithiation. In addition, severe cracks appear in the pristine SMP electrode (Figure S9c), and the SMPs are severely broken due to pulverization (Figure S9d). However, the integrity is well maintained in the 0.2ANF-SMP electrode (Figure S9g and S9h). Therefore, combining the results of electrochemical performance and the thickness changes of electrodes, the inhibition effect of the ANF coating on the volume expansion of SMPs is evident. The sample 0.2ANF-SMP may be the formula of choice, as the experiment fact indicates that an inappropriate ANF loading, either too high or too low, may not well balance the inhibition of volume expansion and the maintenance of electrochemical performance.

5. Capacity and ICE of ANF-SMP

Table. S1 Capacity and ICE of SMP coating with different mass loading of ANFs.

Sample	Discharge capacity (mAh g^{-1})	Charge capacity (mAh g^{-1})	ICE (%)
SMP	1344.04	1127.42	83.88
1ANF-SMP	1409.3	1176.05	83.45
0.2ANF-SMP	1358.76	1137.67	83.73
0.1ANF-SMP	1485.18	1244.3	83.79

Table. S2. Characteristic parameters obtained from XPS analysis of ANF-SMP.

	C-C/C=C	C=O	C-O	N-C=O
SMP (wt%)	35.0	8.8	51.5	4.7
0.1ANF-SMP (wt%)	36.2	9.4	49.6	4.8
0.2ANF-SMP (wt%)	37.8	9.7	47.5	5.0
1ANF-SMP (wt%)	44.4	10.7	39.4	5.5

Table. S3. A performance comparison of Si-based anodes with our work.

Sample		ICE（%）	Capacity (mAh g^{-1})	Volume expansion (%)	Cycles and capacity retention	references
SCNT-NH_2-L	SiMP	89.70	3632	37.6	50, 70%	[3]
OS-PAA	SiNP	62.39	3441.7	78.3	100, 40.28%	[4]
Mp-Si@Si@G	SiMP	88.7	2834	13.7	300, 43.97%	[5]
DSM-Si-6	SiMP	76.66	1606	154.0	100, 90%	[6]
PAA-PEG-Ca^{2+}	SiNP	91.07	3491.1	51.1	800, -	[7]
SiC-SH-ECH	SiNP	76.97	490.1	237.9	800, 69.4%	[8]
Si@G@PDA-C	SiNP	74.55	1416	-	400, 88.5%	[9]
PPTU/Si	SiNP	80.1	3950	18	300, 76.7%	[10]
Si@PAA-B-HPR	SiNP	95.71	2403	8.63	500, 50.14%	[11]
0.2ANF-SMP	SiMP	83.73	1358.76	41.31	100, 90.7%	This work

6. Reference

1. M. Yang, K. Cao, L. Sui, Y. Qi, J. Zhu, A. Waas, E. M. Arruda, J. Kieffer, M. D. Thouless and N. A. Kotov, *ACS Nano*, 2011, **5**, 6945-6954.
2. W. Tang, Q. Liu, N. Luo, F. Chen and Q. Fu, *Composites Science and Technology*, 2022, **225**, 109479.
3. Z. Sun, J. Zhu, C. Yang, Q. Xie, Y. Jiang, K. Wang and M. Jiang, *ACS Applied Materials & Interfaces*, 2023, **15**, 12946-12956.
4. J. Li, J. Fleetwood, W. B. Hawley and W. Kays, *Chemical Reviews*, 2021, **122**, 903-956.
5. Y. He, X. Yu, Y. Wang, H. Li and X. Huang, *Advanced Materials*, 2011, **23**, 4938-4941.
6. B. Zhang, D. Liu, H. Xie, D. Wang, C. Hu and L. Dai, *Journal of Power Sources*, 2022, **539**, 231591.
7. X. Hu, K. Liang, J. Li and Y. Ren, *Materials Today Communications*, 2021, **28**, 102530.
8. J. Wang, L. Liao, H. R. Lee, F. Shi, W. Huang, J. Zhao, A. Pei, J. Tang, X. Zheng, W. Chen and Y. Cui, *Nano Energy*, 2019, **61**, 404-410.
9. Y. Yang, C. Ni, M. Gao, J. Wang, Y. Liu and H. Pan, *Energy Storage Materials*, 2018, **14**, 279-288.
10. X. Jiao, X. Yuan, J. Yin, F. Boorboor Ajdari, Y. Feng, G. Gao and J. Song, *ACS Applied Energy Materials*, 2021, **4**, 10306-10313.
11. H. Wang, D. Wei, B. Zhang, Z. Ji, L. Wang, M. Ling and C. Liang, *ACS Applied Materials & Interfaces*, 2021, **13**, 37704-37712.
12. Y. Yan, Z. Xu, C. Liu, H. Dou, J. Wei, X. Zhao, J. Ma, Q. Dong, H. Xu, Y.-s. He, Z.-F. Ma and X. Yang, *ACS Applied Materials & Interfaces*, 2019, **11**, 17375-17383.
13. Y. Su, X. Feng, R. Zheng, Y. Lv, Z. Wang, Y. Zhao, L. Shi and S. Yuan, *ACS Nano*, 2021, **15**, 14570-14579.
14. Z. H. Xie, M. Z. Rong and M. Q. Zhang, *ACS Applied Materials & Interfaces*, 2021, **13**, 28737-28748.